Optics Communications 285 (2012) 3453–3458

Contents lists available at SciVerse ScienceDirect

Optics Communications

journal homepage: www.elsevier.com/locate/optcom

Submicron-scale spatial compression of light beam through two-stage photonic crystals spot-size converter

N. Cui [a,b], J. Liang [a], Z. Liang [a], Y. Ning [a], W. Wang [a,*]

[a] State Key Laboratory of Applied Optics, Changchun Institute of Optics, Fine Mechanics and Physics, Chinese Academy of Sciences, Changchun, Jilin 130033, China
[b] Graduate School of the Chinese Academy of Sciences, Beijing 100039, China

ARTICLE INFO

Article history:
Received 9 April 2011
Received in revised form 30 March 2012
Accepted 30 March 2012
Available online 12 April 2012

Keywords:
Photonic crystals
Photonic integrated circuits
Nanowire waveguide

ABSTRACT

Photonic crystals spot-size converter that achieved the controlling of the spot-size through two-stage conversions was proposed. The pre-conversion depended on the efficient coupling between the high quality factor resonator and photonic crystal waveguide. Nearly unity transmission efficiency of the pre-conversion can be achieved through optimizing the radii of the rods located surrounding the resonator. Nanowire waveguide with width of 0.14 μm at a distance 1.05 μm from the resonator was introduced to realize the second stage conversion. Through two-stage conversions, the light beam width was converted to 0.16 μm. The transmission efficiency and conversion ratio reached to 94.6% and 14.875 respectively in theory.

1. Introduction

Photonic crystals (PCs), a kind of dielectric structures whose dielectric constant varies periodically in space, have attracted extensive interest in recent decades because of their unique ability on controlling the flow of light. By introducing line defect into PCs, it is possible to build photonic crystals waveguides (PCWG) that can support certain propagating waveguide modes [1–4]. We can also construct resonators that can localize photons in ultra small volume through introducing point defect [5–7]. On the basis of the efficient PCWG and PCs resonators, some PCs devices such as PCs all-optical switches [8,9], PCs couplers [10–12] and PCs filters [13,14] are realized.

PCs are envisaged as main candidates to implement the future integrated photonic/optical circuit because of the compact structure and appealing optical functionalities. In constructing the integrated photonic/optical circuit, the compression and nanofocusing of light beam that can achieve highly efficient coupling between photonic guided-wave devices with different cross-sectional dimensions are indispensable. The key parameters to access the spot-size conversion and nanofocusing are the transmission efficiency, the conversion ratio and the spot size. The conventional sopt-size converter (SSC) [15–19] on the taper structure such as the taper fiber or taper waveguide [20–22]. Then, the taper structure based SSC suffers serious radiation loss and mode mismatching owing to the change of the width [23]. To restrain the loss, the taper structure is usually designed with small taper angle, which incurs large volume consequently. Some solutions such as introducing the parabolic lens [24] and telescope optical system [23] were proposed. However, the introducing of optical components will lead to complicated structure and enlarge the volume. Moreover, these optical components such as parabolic lens are limited by the diffraction of light in the scale of submicron. Thus, an approach that can realize the efficient conversion of the spot-size and nanofocusing of the lightwaves beam in submicron scale with compact structure and small volume is an issue of crucial importance in constructing the photonic/optical circuit.

In this paper, the proposed SSC is based on the coupling between PCs and nanowire waveguide (NWG). Compared with the conventional SSC, the NWG based SSC relies on the efficient coupling among PCWG, PCs resonator and the NWG, which avoids the use of the taper structure. Therefore, the NWG based SSC is more compact and smaller. Additionally, the PCs and NWG are popular components in the integrated photonic/optical circuit, which exhibits excellent compatibility. The NWG based SSC is composed of the incident waveguide (W5 PCWG), the pre-conversion part, the second stage conversion part and the output waveguide (silicon NWG). Through integrating the above components, a highly compact and efficient approach is achieved. The pre-conversion relies on the efficient coupling between PCWGs and the high-Q PCs resonators, which is widely studied [12,25,26] owing to its profound impact on the integrated optics. For the pre-conversion, lightwaves are coupled into W1 PCWG from the incident waveguide (W5 PCWG) via the high-Q (quality factor) PCs resonator. Lightwaves are compressed because the light experiences waveguides with different cross-sectional dimensions. The second stage conversion relies on the coupling between W1 PCWG and NWG whose large index provides tight optical confinement for low-order modes [27–29]. Besides the conversion of the spot-size, SSC also realizes the efficient coupling between PCs devices and NWG, which provides an

* Corresponding author.
E-mail address: wangwbt@126.com (W. Wang).

0030-4018/$ – see front matter © 2012 Elsevier B.V. All rights reserved.
doi:10.1016/j.optcom.2012.03.030

approach to access the integration of PCs devices and conventional optical components such as the gratings and the lenses. Because the light wave is reversible, SSC can also achieve the propagation from the NWG to PCs devices and realize the expansion of the incident beam. In comparison with the taper structure, SSC shows the following advantages: high conversion ratio, high transmission efficiency, compact structure, monolithic integration and much smaller volume.

2. Pre-conversion

As shown in Fig. 1, the pre-conversion of SSC is composed of the incident waveguide, the high-Q PCs resonator and the output waveguide. Through the high-Q resonator, lightwaves are coupled into the output waveguide with cross-sectional dimension smaller than that of the incident waveguide. The amplitude of the selected wave is denoted by a. The amplitudes of the incoming or outgoing waves for the resonator are denoted byS_1,S_{-1},S'_1,S'_{-1} respectively. The squared magnitude of the amplitude is equal to the energy in the mode. According to the coupling theory [12,20,21,24], the time evolution of the resonator is described as:

$$\frac{da}{dt}=\left(j\omega_0-\frac{\omega_0}{Q_0}-\frac{\omega_0}{2Q_b}-\frac{\omega_0}{2Q_a}\right)a+e^{j\theta_a}\sqrt{\frac{\omega_0}{2Q_a}}S'_1+e^{j\theta_b}\sqrt{\frac{\omega_0}{2Q_b}}S_1. \tag{1}$$

Where ω_0 is the resonant frequency of the resonators, Q_0 is the Q factor of the resonator due to intrinsic loss of the cavities. Q_a and Q_b are the Q factors related to the rates of decay into the incident waveguide and the output waveguide respectively.

At the resonance frequency, the transmission efficiency of the SSC can be written as:

$$\eta=\left|\frac{S'_{-1}}{S_1}\right|^2=\left(\frac{Q_0Q_b+2Q_aQ_b}{Q_0Q_a+Q_0Q_b+2Q_aQ_b}\right)^2. \tag{2}$$

It can be found from Eq. (3) that the transmission efficiency is sensitive to Q_a, Q_b and Q_0.

As shown in Fig. 2, the transmission efficiency of the pre-conversion declines as increasing Q_a and Q_0. In addition, a large Q_b is advantageous to realize the high transmission efficiency. When the quality factor for the rate decay into output waveguide (Q_b) is much larger than that for the rate decay into the incident waveguide (Q_a) and the intrinsic loss (Q_0), lightwaves are coupled into the output waveguide efficiently.

Fig. 3(a) shows the structure schematic of the pre-conversion. We consider two-dimensional PCs composed of square array silica rods in air with a lattice constant $p=510$ nm. The radius of the rods is $r=0.2p$. Calculated through plan wave expansion method (PWE), it is found the transverse magnetic(TM) photonic band gap of the PCs extends from 0.29 to 0.42. A point defect consisting of a rod with a radius smaller than that of the surroundings is introduced to construct the high-Q micro-cavity, where the radius of the point defect $r_p=0.1p$. Line defects with radius of $r_l=0.1p$ are introduced to construct the incident waveguide (W5 PCWG). The other PCWGs such as the W1, W3 and W7 PCWG and so on can be used as the incident waveguide according the requirement too. Particularly, when the W1 PCWG is used as the incident waveguide, the SSC connect the W1 PCWG and the NWG together, and the SSC is served as an efficient coupling structure between the PCs and the NWG. The selection of the W5 PCWG can enhance the compatibility of the SSC, because that the width of the W5 PCWG used in communication waveband is typically in several micros, which is close to the width of the conventional optical devices, such as the optical waveguide. Additionally, if the wider PCWG was selected, the SSC can be utilized as the incident terminal of the other device to connect the light source and the other functional device. The wider incident width can reduce the requirement of the pro-focusing and collimation. The selected wavelength is 1550 nm. The relevant structure parameters were realistically estimated for structures fabricated in silicon-on-insulator (SOI) to construct PCs slab. The simulation was performed using finite difference time domain method (FDTD) method with perfectly matched layer (PML) absorbing boundary condition. To investigate the transmission characteristics of the pre-conversion, we introduce two monitors to record the intensity of the output beam and the reflection loss, as shown in Fig. 3(a). The pre-conversion is excited with Gaussian wave. We located the source inside the structure because that the input coupling issue is kept outside of the scope of the paper.

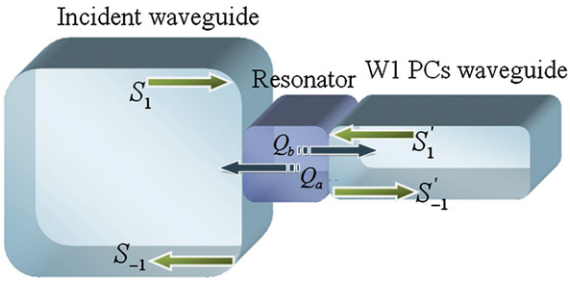

Fig. 1. The schematic of the pre-conversion. The pre-conversion of the SSC relies on the efficient coupling between PCWG and PCs high-Q resonator.

As revealed in Fig. 2, to achieve the efficient coupling, we need to restrain Q_0 and Q_a, while enhance the rate decay into output waveguide (Q_b). For appropriately designed resonators and large enough surrounding photonic crystal materials, the intrinsic loss of the cavity is attributed to the reflection loss at the interface between the interior and exterior of the cavity [12,30,31]. For the 2D PCs resonators, the intrinsic loss mainly comes from the vertical loss of the lightwaves. One of the best approaches to resolving this problem is the PCs slab [32], in which the lightwaves are confined by total internal reflection. Developing from the PCs slab, the heterogeneous nanowire arrays with a smaller refractive index for the lower section of the wire [32] was theoretically demonstrated more efficient on restraining the vertical loss of the PCs resonator. Therefore, for the 2D rods resonator based PCs devices, the intrinsic loss can be controlled through designing the structure on the PCs slab or with heterogeneous structure. Q_a and Q_b can be modulated through optimizing the radii of the rods located between resonator and incident waveguide/output waveguide (r_1 and r_2) that influence the rate decay into the incident and output waveguide respectively. Fig. 3(b) reveals the normalized transmission efficiency of the SSC as a function of r_1. The normalized intensity of output beam reaches the peak and the value of the reflection loss is relatively low at the point of $r_1=0.04$ μm. Likewise, Fig. 3(c) reveals the curves of the normalized intensity of the output beam and the reflection loss as a function of r_1.when $r_1=0.04$ μm and $r_2=0.06$ μm, the pre-conversion shows a high coupling efficiency.

3. Second stage conversion

The second stage conversion relies on the efficient coupling between the PCWG and the NWG. Combining the two-stage conversions together, the width of lightwaves in z direction can be converted to the submicron-scale. Fig. 4(a) reveals the 3D schematic of the SSC. A silicon NWG with length of l and width of w is embedded into the W1 PCWG. The interval between the point defect of the resonator and the NWG is denoted by d. Similar to the analysis of the pre-conversion, two monitors are introduced to record the intensity of output beam and reflection loss. Fig. 4(b) reveals the relationship of the transmission efficiency vs. the distance d. At the point of $d=1.05$ μm, the normalized intensity of the output beam reaches the peak. Fig. 4(c) gives the FWHM of the output

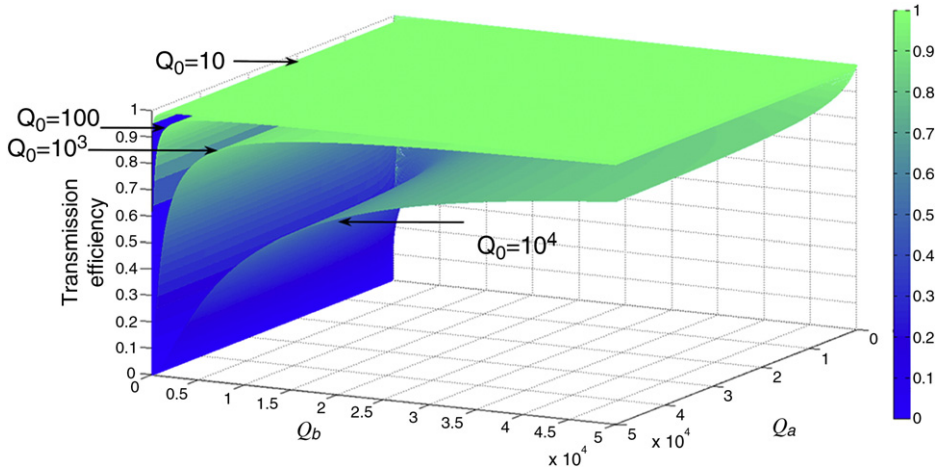

Fig. 2. The transmission efficiency of the pre-conversion as a function of Q_a, Q_b and Q_0. The minimum and maximum ranges of the transmission efficiency plots are indicated as blue and green colors.

beam as a function of the width of the NWG when $d = 1.05$ μm. When $w = 0.10$ μm, the output beam is compressed to the minimum FWHM (about 0.147 μm). Fig. 4(d) shows the curves of the transmission efficiency as a function of the width of the NWG when $d = 1.05$ μm. Four peaks are found when the width of the NWG are 0.085 μm, 0.14 μm, 0.18 μm and 0.195 μm, which give us several choices for the width of the output beam. Herein, considering the FWHM of the output beam and the transmission efficiency, we select the NWG with width of 0.14 μm. Fig. 4(e) shows the transmission efficiency as a function of the length of the NWG. The transmission efficiency exhibits eight peaks when the length of the NWG is 0.73 μm,1.02 μm,1.46 μm,1.75 μm, 2.04 μm,2.4 μm,2.75 μm and 3.06 μm, the coupling system exhibits a high transmission efficiency (all above 90%). However, if the length of the NWG is larger than six times of the lattice period, the transmission efficiency keeps constant (about 70%). The eight peaks of the transmission efficiency give us widely selection of the length of the NWG.

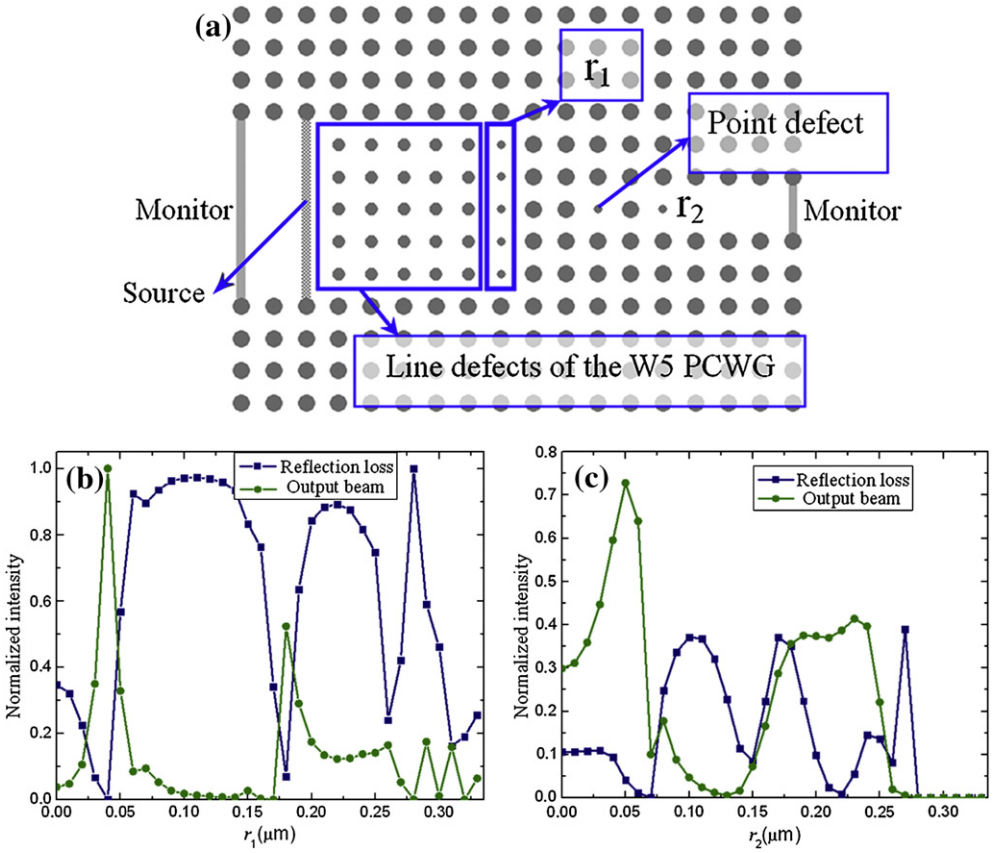

Fig. 3. The structure schematic and transmission characteristic of the pre-conversion. (a) The structure schematic of the pre-conversion. The radii of the rods located between the micro-cavity and the incident/output waveguide (r_1 and r_2) are optimized. (b) The normalized intensities of the output beam and reflection loss as a function of r_1. (c) The normalized intensities of the reflection loss and output beam as a function of r_2. The green and blue lines denote the normalized intensity of the output beam and reflection loss respectively.

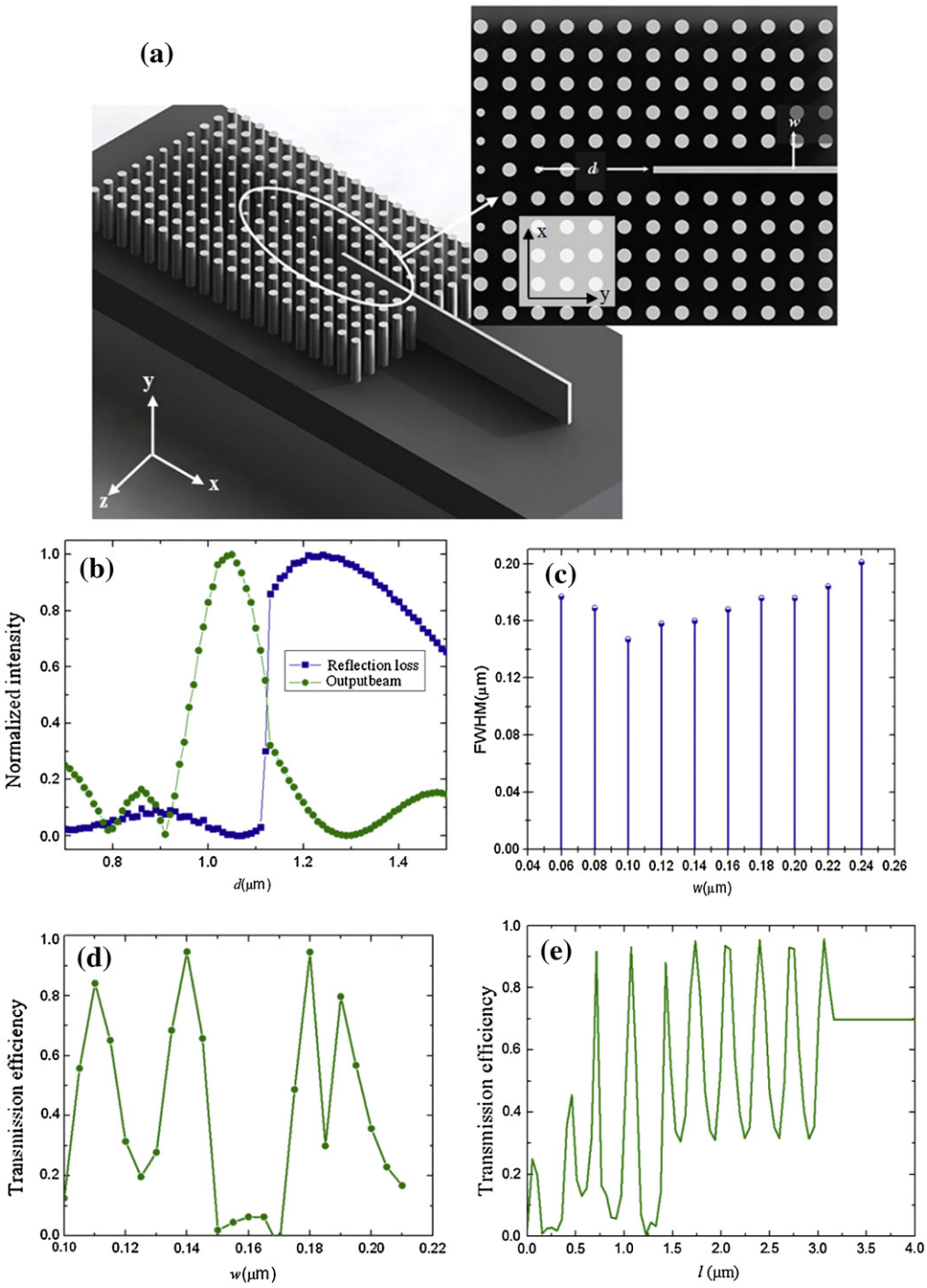

Fig. 4. The schematic and the transmission characteristics of SSC calculated by the FDTD method. (a) 3D schematic of SSC. Inset: the 2D schematic of the second stage conversion. (b) The normalized intensity of the reflection loss and the output beam as a function of the distance between the point defect of the resonator and the NWG. (c) The FWHM vs. the width of the NWG. (d) The transmission efficiency as a function of the width of the NWG. (e) The transmission efficiency as a function of the length of the NWG.

Among the eight peaks, when $l = 6p = 3.06\,\mu m$, the SSC exhibits the highest transmission (94.6%). Therefore, we chose the NWG with length of 3.06 μm as the output waveguide. The other peaks can also be selected, which can provide the transmission efficiency above 90%.

Fig. 5(a) shows the field pattern of the system. The minimum and maximum ranges of the e-filed plots are indicated as blue and red colors. Through the compressing of two-stage conversions, the submicron-scale compression and nanofocusing are achieved. The reflection loss is relatively low and the power is concentrated into the NWG. The power density in the NWG is much higher than that of the incident waveguide. To investigate the compression ratio, we show the power distribution of the output beam in Fig. 5(b). The brown, green, red and blue lines denote the power distribution of incident beam, the beam after the pre-conversion, reflection loss and output beam respectively. Compared to the incident beam, the beam widths compressed by pre-conversion and that of the output beam are much smaller. The curve of the output beam shows a large height to width ratio. In contrast, the reflection loss is extremely

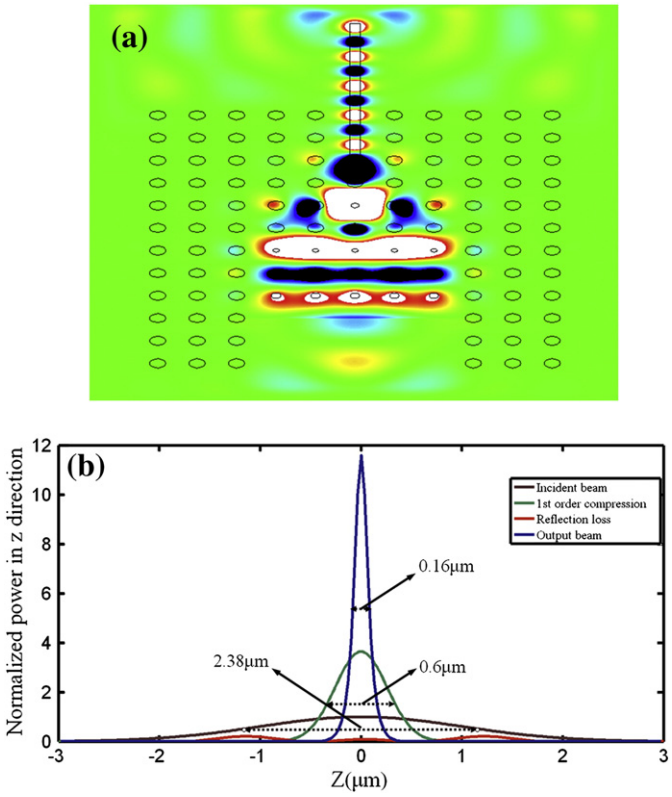

Fig. 5. Fig. 5. The transmission characteristics of the SSC. (a) The field pattern of the SSC. (b) The power distribution in z direction. The brown, green, red and blue lines denote the power distribution of incident beam, the SSC by pre-conversion, reflection loss and output beam respectively.

low. The FWHM of incident beam, pre-converted beam and output beam are 2.38 μm, 0.6 μm and 0.16 μm respectively. Defined compression ratio as:

$$\gamma = {}^{W_i}\!/_{W_0}$$

Where W_i and W_0 are the FWHM of the incident beam and output beam respectively. We gain the compression ratio of the pre-conversion is 3.97 and the total compression ratio of the SSC is 14.875.

Through two-stage beam conversions, the lightwaves is concentrated into the NWG. Thus, the high power density in the NWG is achieved.

4. Conclusions

Photonic crystal SSC was designed. Through the efficient coupling of the PCWG and the NWG, lightwaves were compressed to sub-micron scale. The coupling efficiency of pre-conversion was determined by Q_0, Q_a and Q_b, which can be modulated through optimizing the radii of the rods located surrounding the resonator (r_1 and r_2). When $r_1 = 0.04$ μm and $r_2 = 0.06$ μm, the pre-conversion provides high transmission efficiency. Silicon NWG was embedded into the PCWG to construct the second stage conversion. Considering the transmission efficiency and the compression ratio, the width of NWG was set to 0.14 μm, and the interval between the NWG was set to 1.05 μm. Calculated with FDTD, the light beam was compressed to 0.16 μm. The transmission efficiency and the compression ratio reached to 94.6% and 14.875 respectively. SSC achieves high transmission efficiency and compression ratio with small volume and compact structure, which provides a practical implement for the photonic/optical circuits.

Acknowledgement

The works was supported by the National Natural Science Foundation of China (Grant No. 60877031).

Appendix A

$$\frac{da}{dt} = \left(j\omega_0 - \frac{\omega_0}{Q_0} - \frac{\omega_0}{2Q_b} - \frac{\omega_0}{2Q_a}\right)a + e^{j\theta_a}\sqrt{\frac{\omega_0}{2Q_a}}S_1' + e^{j\theta_b}\sqrt{\frac{\omega_0}{2Q_b}}S_1. \quad (1)$$

$$\begin{aligned} S_{-1}' &= S_1 - e^{-j\theta_b}\sqrt{\frac{\omega_0}{2Q_b}}a \\ S_{-1} &= S_1' - e^{-j\theta_a}\sqrt{\frac{\omega_0}{2Q_a}}a \end{aligned}. \quad (2)$$

$$\eta = \left|\frac{S_{-1}'}{S_1}\right|^2 = \left(\frac{Q_0Q_b + 2Q_aQ_b}{Q_0Q_a + Q_0Q_b + 2Q_aQ_b}\right)^2. \quad (3)$$

References

[1] Jun-ichiro Sugisaka, Noritsugu Yamamato, Makoto Okano, Kazuhiro Komori, Toyohiko Yatagai, Masahide Itoh, Optics Communications 281 (23) (2008) 5788.
[2] Xuan Zhang, Huiping Tian, Yuefeng Ji, Optics Communications 283 (9) (2010) 1768.
[3] Naidi Cui, Jingqiu Liang, Zhongzhu Liang, Jianwei Zhou, Yongqiang Ning, Weibiao Wang, Optics and Precision Engineering 18 (2010) 2549.
[4] Tetsuya Tada, Vladimir V. Poborchii, Toshihiko Kanayama, Microelectronic Engineering 63 (1–3) (2002) 259.
[5] Gangyi Xu, Raffaele Colombelli, Remy Braive, Gregoire Beaudoin, Luc Le Gratiet, Anne Talneau, Laurence Ferlazzo, Isabelle Sagnes, Optics Express 18 (11) (2010) 11979.
[6] Masahiro Nomura, Yasutomo Ota, Naoto Kumagai, Satoshi Iwamoto, Yasuhiko Arakawa, Applied Physics Letters 97 (19) (2010) 191108.
[7] Amir H. Safavi-Naeini, Thiago P. Mayer Alegre, Martin Winger, Oskar Painter, Applied Physics Letters 97 (18) (2010) 181106.
[8] Xiaoyong Hu, Ping Jiang, Chengyuan Ding, Hong Yang, Qihuang Gong, Nature Photonics 2 (2008) 185.
[9] Nakamura Hitoshi, Suginoto Yoshimasa, Kyozo Kanamoto, Yu. Naoki Ikeda, Yusui Nakamura Tanaka, Shunsuke Ohkouchi, Yoshinori Watanabe, Kuon Inoue, Hiroshi Ishikawa, Kiyoshi Asakawa, Optics Express 12 (26) (2004) 6606.
[10] Chengyang Liu, Physics Letters A 373 (34) (2009) 3061.
[11] Ahmed Sharkawy, Shouyuan Shi, Dennis W. Prather, Applied Optics 40 (14) (2001) 2247.
[12] Andrei Faraon, Edo Waks, Drik Englund, Llya Fushman, Jelena Vučković, Applied Physics Letters 90 (7) (2007) 073102.
[13] Ziyang Zhang, Min Qiu, Optics Express 13 (7) (2005) 2596.
[14] Kiazand Fasihi, Shahram Mohammadnejad, Optics Express 17 (11) (2009) 8983.
[15] Hideo Kosaka, Takayuki Kawashima, Akihisa Tomita, Takashi Sato, Shojiro Kawakami, Applied Physics Letters 76 (3) (2000) 268.
[16] Geon Jeong, Donghoo Kim, Junseok Choi, DongHwan Lee, Mahn-Yong Park, Jin-Bong Kim, Hyung Jong Lee, Hyun-Yong Lee, ETRI Journal 27 (1) (2005) 89.
[17] Marko Galarza, Kurt De Mesel, Steven Verstuyft, Cándido Aramburu, Manuel López-Amo, Ingrid Moerman, Peter Van Daele, Roel Baets, Journal of Lightwave Technology 21 (1) (2003) 269.
[18] M.M. Spühler, D. Erni, J. Fröhlich, Journal of Lightwave Technology 30 (1998) 305.
[19] Lianping Hou, Hongliang Zhu, Fan Zhou, Baojun Wang, Jing Bian, Wei Wang, Journal of Crystal Growth 288 (2006) 148.
[20] I. Duport, P. Benech, D. Khalil, R. Rimet, Journal of Physics D: Applied Physics 25 (1992) 913.
[21] Ewold Verhagen, Albert Polman, L. (Kobus) Kuipers, Optics Express 16 (1) (2008) 45.
[22] I.D. Nikolov, Nanotechnology 15 (8) (2004) 1076.
[23] Chun-Wen Chang, Mount-Learn Wu, Wen-Feng Hsieh, IEEE Photonics Technology Letters 15 (2003) 1378.
[24] Atef M. Rashed, Kevin A. Williams, Peter J. Heard, Richard V. Penty, Ian H. White, Optical Engineering 42 (3) (2003) 792.
[25] Yong Xu, Yi Li, Reginald K. Lee, Amnon Yariv, Physical Review E 62 (5) (2000) 7389.
[26] Shanhui Fan, Pierre R. Villeneuve, John D. Joannopoulos, Physical Review Letters 80 (5) (1998) 960.
[27] Lambert K. Van Vugt, Brian Piccione, Ritesh Agarwal, Applied Physics Letters 97 (6) (2010) 061115.

[28] Nathan P. Malcolm, Alex J. Heltzel, Konstantin V. Sokolov, Li Shi, John R. Howell, Applied Physics Letters 93 (19) (2008) 193101.
[29] H.Y. Li, S. Rühle, R. Khedoe, A.F. Koenderink, D. Vanmaekelbergh, Nano Letters 9 (10) (2009) 3515.
[30] M.G. Banaee, Jeff F. Young, Optics Express 16 (25) (2008) 20908.
[31] Yoshihiro Akahane, Takashi Asano, Bong-Shik Song, Susumu Noda, Nature 425 (2003) 944.
[32] Tao Xu, Suxia Yang, Selvakumar V. Nair, H,.E. Ruda, Physical Review B 75 (12) (2007) 125104.